PHYSICAL REVIEW B VOLUME 2, NUMBER 10 15 NOVEMBER 1970

Properties of Spontaneous and Stimulated Emission in GaAs Junction Lasers. II. Temperature Dependence of Threshold Current and Excitation Dependence of Superradiance Spectra

C. J. Hwang
Bell Telephone Laboratories, Murray Hill, New Jersey 07974
(Received 27 March 1970)

The spontaneous and stimulated emission spectral functions are calculated using a band model consisting of the self-consistent densities of states calculated in a previous paper and an optical model with an energy-dependent matrix element and no selection rule for the radiative recombinations. The energy dependence of the matrix element is that for a transition from a parobolic conduction band to an acceptor level and should be a suitable one, because of a small conduction band tail and the occupancy of most of the holes in the vicinity of the acceptor ionization energy. General properties, such as the spontaneous emission band shape, the gain-current relationship, and the temperature dependence of current required to maintain a given gain are compared with those calculated without band tails and with band tails given by Kane's model. Considerable differences are found among various models and these are discussed. The calculations on the temperature dependence of the threshold current and the current dependence of the superradiance spectra are then applied to GaAs-diffused diodes with substrate doping of 3×10^{18} cm^{-3}, taking into account the temperature dependence of the cavity loss and the non-uniform acceptor distribution in the p layer. Detailed comparison with experimental data is made and good quantitative agreement is obtained in both cases, giving strong support to our conclusions concerning the band-tail structure.

I. INTRODUCTION

In this paper, we use the self-consistent densities of states calculated in paper I[1] to compute the spontaneous and stimulated absorption spectra. The band-gap shrinkage, due to the effect of Coulomb and exchange interactions[1] and the energy dependence of the matrix element, both of which were not considered in previous calculations, are taken into account The calculated general properties of the spontaneous and stimulated emission such as the spontaneous emission band shape, the gain-current relationship, and the temperature dependence of the excitation required to maintain a given gain are compared with those calculated from a parabolic and Kane's densities of states.[2] It is found that the different expressions for the density of states yield considerably different results for these properties. In order to determine the electron distribution in the p layer with nonuniform impurity distribution, we calculate the electron diffusion constant and diffusion length for a given compensation and injection level. The above calculations are finally applied to diffused diodes with substrate doping of 3×10^{18} cm^{-3}. We present and compare in great detail the calculated and experimental results of the two most important properties of a laser, i.e., the temperature dependence of the threshold current and the spontaneous emission spectra in the superradiance region. Good quantitative agreement is found in both cases, thus giving strong support to our conclusion on the densities of states in the active region as calculated in paper I.

II. CALCULATION OF THE SPONTANEOUS AND STIMULATED SPECTRAL FUNCTIONS

A. Optical Model for the Radiative Recombination

In an optically isotropic medium in which radiative transitions take place between states in the conduction band and the states in the valence band, the spontaneous rate of photon emission per unit volume and per unit energy at photon energy $h\nu$, $\gamma_{\rm spon}(h\nu)$, is given by[3]

$$\gamma_{\rm spon}(h\nu)=\int B'\rho_v(-E)\left[1-f_v(E)\right]\times\rho_c(h\nu-E_g+E)f_c(h\nu-E_g+E)\,dE, \qquad (1)$$

where ρ_c and ρ_v are, respectively, the conduction and valence band densities of states, f_c and f_v are the Fermi functions for electrons in the conduction and valence bands and B' is the recombination constant (in cm^3/sec) for an electron in the conduction band recombining with a hole in the valence band. In Eq. (1), E is measured positively upward from the valence band edge. Assuming that the thermalization times for electrons and hole are short compared with their recombination lifetimes, two quasi-Fermi levels E_{fe} for electrons and E_{fh} for holes can be introduced. These are defined as positive when measured into the conduction and valence bands from the respective band edges (see paper I for the definition of band edge). The Fermi function for electrons in the valence band can then be expressed as

$$f_v(E)=\left(1+e^{(E+E_{fh})/kT}\right)^{-1}, \qquad (2a)$$

and for electrons in the conduction band,

$$f_c(h\nu - E_g + E) = (1 + e^{(h\nu + E - E_g - E_{fe})/kT})^{-1}, \qquad (2b)$$

where T is the absolute temperature and k is Boltzmann's constant.

The absorption coefficient $\alpha(h\nu)$ is related to $\gamma_{spon}(h\nu)$ and the difference between the electron and hole quasi-Fermi levels ΔE_f as follows[3]:

$$\alpha(h\nu) = \pi^2 c^2 \hbar^3 n^{-2} (h\nu)^{-2} \gamma_{spon}(h\nu) e^{(h\nu - \Delta E_f)/kT - 1}, \qquad (3)$$

where

$$\Delta E_f = E_{fe} + E_g + E_{fh}, \qquad (4)$$

$n = 3.6$ is the refractive index at $h\nu$, and c is the velocity of light. We see that when $h\nu < \Delta E_f$, α is negative and an amplification of light results. Accordingly, we shall define the maximum of the negative $\alpha(h\nu)$ as the gain g. The threshold condition for stimulated emission is then given by $g = \alpha_L$, where α_L is the total cavity loss.

In order to calcluate $\gamma_{spon}(h\nu)$ and hence $\alpha(h\nu)$, we need to know the recombination constant B'. Referring to Fig. 3 of paper I we see that the conduction band tail is negligibly small and that the valence band tail spreads in the vicinity of an energy E_A very close to a shallow acceptor ionization energy in GaAs. In most cases, and particularly at higher temperatures, E_{fh} is located in the valence band tail (see Fig. 4 of paper I) and E_{fe} is located in the parabolic portion of the conduction band. We shall therefore assume that a transition from a conduction band to the valence band can be approximated by the case in which the transition is from the parabolic conduction band to the shallow acceptor state with ionization energy E_A. Dumke[4] has derived the matrix element for this case from which B' can be written as

$$B' = B[1 + (a^* k)^2]^{-4}, \qquad (5)$$

where $B = 7.5 \times 10^{-10}$ cm^3/sec (corresponding to $E_A = 34$ meV)[2,3] is the recombination constant used in all the previous no-selection-rule calculations,[2,3,5,6] $a^* = \epsilon\hbar^2/(m^* e^2)$ is the acceptor orbit radius, $m^* = 2\epsilon^2\hbar^2 E_A/e^4$, $k = (2m_c^* E_c'/\hbar^2)^{1/2}$, and E_c' is measured from the point where $\rho_c = 0$. This point is hard to define since the conduction band tail decreases indefinitely with energy. In the present case, however, the conduction-band-tail density of states decreases rapidly into the gap and ρ_c reduces to a value smaller than 10^{14} cm^{-3} eV^{-1} within E_c^c below the band edge, where E_c^c is the amount of band-edge shift due to Coulomb interaction.[1] We shall thus set $E_c' = E_c^c + (h\nu - E_g + E)$, where E is measured from the valence band edge.

Combining Eqs. (1) and (5), we see that the recombination rate is smaller for electrons occupying states with energy greater than $E_c' > (m^*/m_c^*) E_A$. All the previous calculations[2,3,5,6] neglected this effect and may therefore overestimate the total recombination rate at higher temperatures due to the increase in population at high values of E_c'. Other than this, the use of Eq. (5) for B' is not really justified since states in the tail may have different wave functions than do states in the parabolic portion of the band. In addition, the states far deep in the tail may have more localized wave functions than do those in the upper part of the tail. These differences will certainly affect the matrix element and hence the recombination constant, but there appears to be no quantitative results on heavily doped crystals on which to base a better approximation than the one given in Eq. (5). The approximation resulting from using Eq. (5) for B', should, however, be a reasonable one for lasers with a total loss $\alpha_L \geq 50$ cm^{-1} above 150 °K near the threshold, since E_{fe} and E_{fh} are then located in the parabolic portion of the conduction band and the valence band tail, respectively.

The optical model used in this calculation is valid provided that the net hole concentration in the p layer does not exceed 6×10^{18} cm^{-3}. This is because the states perturbed by the impurities employ the phase space provided by the unperturbed parabolic band states and the available phase space is effectively exhausted at this indicated hole concentration, as was pointed out by Dumke.[4] Our net hole concentrations are all below this limit.

B. Injection Current Density

In presenting our results, it is useful to give the quantities of interest in terms of the current density or the injected electron concentration. We shall use both depending on whichever is more appropriate even though they are related. For convenience and for comparison with results calculated using other models, we define a nominal current density J_{nom} as

$$J_{nom} = 1.602 \times 10^{-23} \mathcal{R}, \qquad (6)$$

where

$$\mathcal{R} = \int_0^\infty \gamma_{spon}(h\nu)\, d(h\nu)$$

is the total recombination rate. The quantity J_{nom} is thus the current density which must flow to maintain the total recombination rate $\mathcal{R}$ cm^3/sec in a layer of 1 μ thick if the internal quantum efficiency η is equal to 100%. Note that $J_{nom} \neq B'NP$, where N and P are the electron and hole concentrations, respectively, since B' is energy dependent. If the p region of the junction is nonuniform in impurity distribution and the hole injection is small compared to the electron injection, the total current density flowing through the device is

$$J = [1.602 \times 10^{-23} \int_0^d \mathcal{R}(x)]/(\eta\eta_1), \qquad (7)$$

where d is the width of the p region and is equal to the junction depth of the diffused layer and x is the distance measured from the junction toward the p region. In Eq. (7), η_1 is the fraction of total electrons actually taking part in the recombination, since it is possible in a shallow junction that some electrons may reach the surface of the p layer before recombining with the holes in the p region. The quantity η_1 can be expressed as

$$\eta_1 = N(0)/[N(0) - N(d)], \tag{8}$$

where $N(0)$ and $N(d)$ are the electron concentration at $x=0$ and $x=d$, respectively. The quantity $N(d)$ can be calculated from the electron diffusion constant in the p region. The threshold current density J_t is defined as the current density required to maintain a given gain which is equal to the total loss of the laser, taking into account the factor Γ due to the incomplete confinement of the mode propagating along the active layer[2]:

$$J_t = J/\Gamma. \tag{9}$$

All the computations were performed on a CDC-6600 computer. The integration grid is 0.5 meV for calculating $\gamma_{\text{spon}}(h\nu)$, but 5 meV for calculating $\mathcal{R}$ because of the relatively smooth variation of $\gamma_{\text{spon}}(h\nu)$ with $h\nu$.

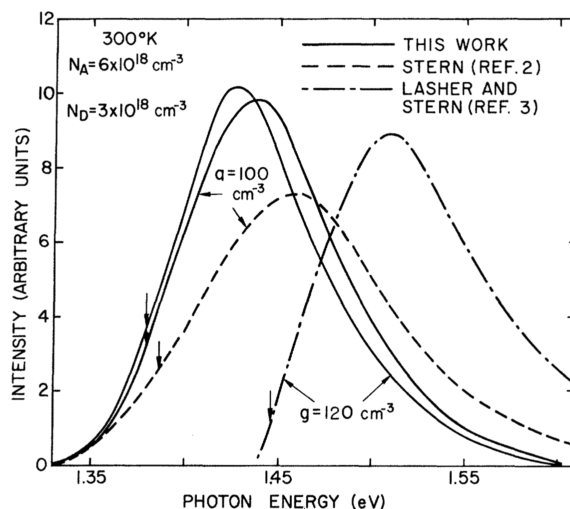

FIG. 1. Spontaneous emission spectra at injection levels required to maintain a gain of 100 and 120 cm^{-1} for recombination in a region with 3×10^{18} donors and 6×10^{18} acceptors per cm^3. The results obtained by other workers using parabolic and Kane's expressions for the density of states are also plotted for comparison. All the curves have been normalized to unit area. The arrows mark the energies at which the negative absorption has its peak.

C. Results and Discussion

We first show, in Fig. 1, as an example the spontaneous emission spectra $\gamma_{\text{spon}}(h\nu)$ calculated for 300 °K at excitation levels corresponding to $g = 100$ cm^{-1} and 120 cm^{-1}. For comparison, we also plot the results of Lasher and Stern,[3] and Stern[2] as calculated without band tails and with band tails given by Kane's model. Each curve has been normalized to its own $\mathcal{R}$ and the arrow marks the energy at which $-\alpha$ has its maximum. The differences in the peak position, the band shape, and the bandwidth are apparent. If the band shift due to the exchange and Coulomb interactions are neglected as in the calculations of Lasher and Stern, and Stern, the peak position of $\gamma_{\text{spon}}(h\nu)$ would be very close to that calculated by Lasher and Stern. Our calculation thus shows that it is not the band tails, but the carrier-carrier and carrier-impurity interactions which effectively reduce the band gap and bring the predicted peak energy smaller than the band-gap energy of the pure crystal. This is contrary to the case of Stern's calculation in which the lowering in peak energy is solely due to band-tail effect. The fact that Stern's curve occurs at lower energy and has larger bandwidth reflects the long- and large-tail density of states inherent in Kane's theory, as was pointed out in paper I. The slope of the low-energy tail of our spectrum is somewhat in between those obtained by Lasher and Stern, and Stern but the high-energy tail decreases faster than both. Since the low-energy tail is due to transitions involving states with $E < (m^*/m_c^*)E_A$, we have $B \simeq B'$ and the slope thus reflects the structure of our density of states in the tails which lie in between Kane's theory and the parabolic function. On the other hand, $B' < B$ for $E > (m^*/m_c^*)E_A$, and hence our high-energy tail decreases faster than those calculated with B.

In Fig. 2, we plot the dependence of gain g on nominal current density J_{nom} for donor and acceptor concentrations of $N_D = 1\times10^{18}$ cm^{-3} and $N_A = 4\times10^{18}$ cm^{-3} for several temperatures below 300 °K. Also plotted for comparison are the results of Lasher and Stern,[3] and Stern.[2] We see that, for a given gain, our J_{nom} is in between that obtained by Lasher and Stern[3] and that obtained by Stern[2] for $T \le 160$ °K but is smaller than both at 300 °K. The calculated results thus strongly depend on the density of states and the recombination constant used. At low temperatures ($T \le 160$ °K) and in the gain region of $g < 200$ cm^{-1}, most of the electrons populate the states with energy less than $(m^*/m_c^*)E_A$. In this case, $B' \simeq B$, the difference between our results and those of other workers should be due mainly to the difference in the density of states. Since our density-of-states function lies somewhat in between Kane's expression and the parabolic function, our results here clearly demonstrate the large effect of band-tail structure on the g versus J relation. At high temperatures ($T > 160$ °K), more electrons are

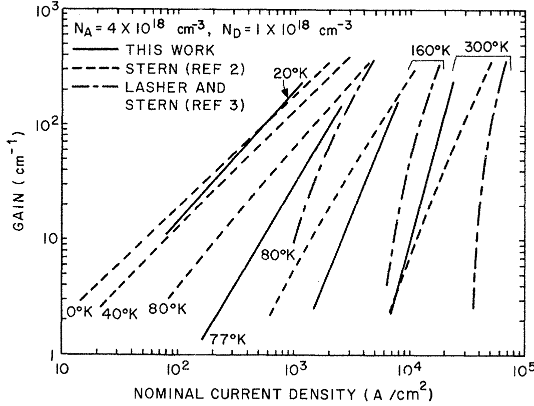

FIG. 2. Variation of gain with nominal current density defined in Eq. (6) for recombination in a region with 1 $\times 10^{18}$ donors and 4×10^{18} acceptors per cm^3. The results obtained by other workers are also plotted for comparison. b in the equation $g \propto J^b_{nom}$ is equal to 1.65 at 77 °K and 3.7 at 300 °K as compared to the respective experimental values of 1.4 and 3.1 given in Ref. 9.

in the high-energy ($E'_c > (m^*/m^*_c)E_A$) states, and the current density J_{nom} calculated with B' should be smaller than J_{nom} calculated with B. On the other hand, since the region of negative absorption occurs at $h\nu < \Delta E_f$, i.e., the transitions are mostly from electron states below E_{fe}, and E_{fe} is equal or smaller than $(m^*/m^*_c)E_A$, the gain will not be appreciably affected by replacing B by B'. Therefore, using B instead of B' at high temperatures will overestimate the current required to maintain a given gain. The fact that our J_{nom} at 300 °K is smaller than that obtained by Stern[2] indicates that the energy dependence of B' is more important than the effect of the band tails on the calculated results at this temperature.

An almost exact relation of the form $g \propto J^b_{nom}$ is obtained at all temperatures below 300 °K for different donor and acceptor concentrations, but with compensation of $N_A - N_D = 3\times10^{18}$ cm^{-3}, where b is a constant ranging from about 1 at low temperatures ($T \lesssim 20$ °K) to about 3 at 300 °K depending on the total impurity concentration. In the past, it has been suggested[7] that g varies linearly with current at all temperatures. This was derived from the length dependence of the threshold current using the threshold equation[7]

$$J_t \beta = (1/l) \ \ln(1/R) + \alpha_l = \alpha_L , \qquad (10)$$

where l is the length of the laser, R is the reflectivity of the mirror, α_l is the internal loss of the laser and β is the gain factor. In the analysis of the experimental data, it has been assumed that α_l is length independent and a plot of J_t against $1/l$ then leads to the conclusion that $g \propto J$. Recent experiments on the length dependence of the threshold and efficiency by Susaki[8] and Goodwin,[9] however, indicate that α_l does depend on d, and a self-consistent analysis of the experimental data shows that $g \propto J^b$ indeed holds.[9] Our value of $b = 1.65$ at 77 °K and $b = 3.7$ at 300 °K is in reasonable agreement with Goodwin's values of $b = 1.4$ at 77 °K and $b = 3.1$ at 300 °K for lasers with $N_D = 1\times10^{18}$ cm^{-3}. Note that the log-log plot of Stern's g versus J_{nom} data above 160 °K is slightly nonlinear.

The temperature dependence of the excitation required to reach a gain of 100 cm^{-1} is shown in Fig. 3. Results obtained by other workers are also plotted for comparison. Unger's curve[5] was obtained using a parabolic density of states and an active-region hole concentration determined from the condition of maximum recombination rate. If we used B instead of B' in the calculation, our curves would lie in between those obtained by Stern,[2] and Lasher and Stern,[3] and Unger.[5] The crossover of two curves with different dopings seen in the calculations of Stern[2] and Unger[6] is also predicted in this calculation. The above two observations are also manifestations of the effect of band tails.

The curves in Fig. 3 represent the temperature dependence of the threshold current density for a laser with a compensation of $N_A - N_D = 3\times10^{18}$ cm^{-3} in the active region and a total loss of $\alpha_L = 100$ cm^{-1}. The calculations with B as the recombination constant thus all show a nearly $J_t \propto T^3$ relationship regardless of whether the band tails are included or not. Our curve shows a less steep temperature variation at high temperature since B' is used in the calculation. Previous calculations[4,10] were

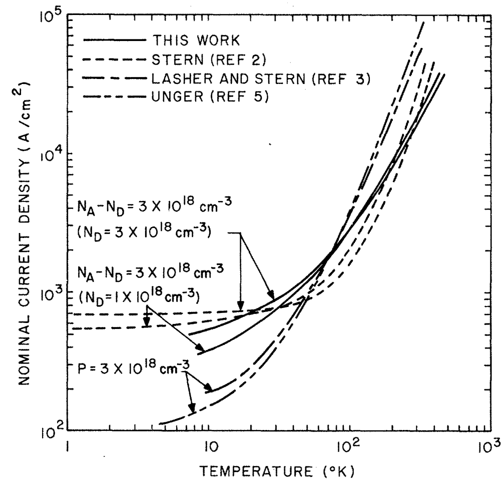

FIG. 3. Temperature dependence of the nominal current density required to reach a gain of 100 cm^{-1} for two compositions with $N_A - N_D = 3\times10^{18}$ cm^{-3}. Curves calculated from other models are also shown for comparison.

aimed at obtaining a strict T^3 law in order to account for the experimental observations. However, recent experiments[11,12] show that an exponential law of the form $J_t \propto e^{T/T_0}$, where T_0 is a constant, is even more frequently observed. As will be seen in Sec. III, our results agree quantitatively with this exponential behavior when the temperature dependence of the total loss α_L is taken into account. It is interesting to note that the calculations with or without band tails, but with no selection rule and constant matrix element, all predict an approximate T^n relationship, where n is between 2 and 3, even though the absolute values of the current densities at a given temperature are different. Since, from Eqs. (1) and (4), the temperature dependences of $\mathcal{R}$ and $\alpha(h\nu)$ are mainly determined by the temperature variation of the Fermi levels, this similar J_{nom} versus T for all calculations can be qualitatively understood from the similar temperature dependence of the Fermi levels shown in Fig. 4 of paper I.

III. COMPARISON WITH EXPERIMENTS

A. Experimental

The diodes were made by Zn diffusion into 3×10^{18} cm^{-3} Te-doped substrates from two different ingots. The diffusion runs were performed at 800 °C for 3 h and a junction depth of 2.1 μ was obtained in each case. The diffusion source was composed of a ratio of approximately Ga: As: Zn = 78.4: 20: 1.6 by atomic fraction. The diffusion profile was not measured directly, because of the shallow nature of the junction. We computed the diffusion profile, independently from the estimated diffusion constant and the surface concentration, and the profile gradient near the junction from capacitance measurements. Since the precise diffusion condition from this source at this temperature is not known, the diffusion constant and the surface concentration cannot be determined. However, one can estimate these two parameters from the existing published works by extrapolation or interpolation. The arsenic pressure at 800 °C for this composition is estimated by extrapolation to be 1×10^{-5} atm from Shih's work.[13] Since the Zn surface concentration at this pressure and below is not sensitive to the arsenic pressure,[14] we estimate our surface concentration to be about 9×10^{18} cm^{-3} from an extrapolation of the data of Chang[15] and Casey *et al.*,[16] which is appropriate for diffusion from a 2% Zn, Ga-Zn alloy source. The diffusion coefficient at this surface concentration can be assumed to be concentration independent[17,18] and can thus be calculated from the known junction depth, the substrate doping, and the surface concentration by using a complementary error-function profile. The value of D so determined is 2.35×10^{-12} cm^2/sec. In Fig. 4, we plot the calculated profile

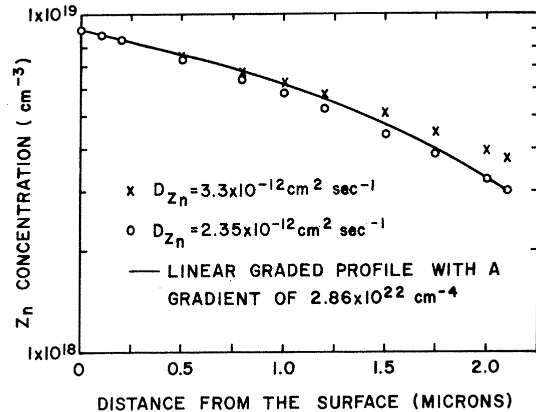

FIG. 4. Acceptor distribution profiles in the p layer for the lasers used in this study. The diffusion was carried out at 800 °C for 3 h from a source composed of Ga : As : Zn = 78.4 : 20 : 1.6 (by atomic fraction) into a 3×10^{18} cm^{-3} n-type GaAs substrate.

(open circles) using this D value and 9×10^{18} cm^{-3} as the surface concentration. The crosses corresponding to a diffusion constant of 3.3×10^{-12} cm^2/sec are also plotted in order to demonstrate the sensitivity of the profile to the diffusion constant. The two profiles are seen to be very close except near the junction. Also in Fig. 4, we plot (solid curve) the linearly graded profile up to the surface, with a gradient of 3×10^{22} cm^{-4} as determined from the capacitance measurements. It is seen that the estimated Zn distribution curves from different measurements agree fairly well. For simplicity, we shall use the linearly graded profile in the later analysis.

The diffused slice was fabricated into laser structures with stripe geometry contacts of dimensions 13 μ (width)$\times$380 μ (length) on the p layers.[19] The temperature dependence of the threshold current was determined by mounting the laser on a coldfinger immersed in liquid nitrogen. The lasers were excited by a 150×10^{-9} sec pulse with a repetition rate of 50 pulses per sec, to avoid heating up the diode. Since the pulse length is much longer than the total lifetime of the electrons, we can regard the excitation as a steady-state case during each pulse. The temperature range was from 80 to 300 °K. The threshold current was taken as the value at which a sudden burst of light could be seen from a snooper scope.

The laser loss α_l was determined by Dyment of this laboratory[20] to be $\alpha_l = 25$ cm^{-1} at 80 °K and $\alpha_l = 120$ cm^{-1} at 300 °K. The variation of α_l with temperatures in between is assumed exponential as shown in the lower part of Fig. 5. The uncertainty in the calculated threshold current resulting from this assumption is less than 10% since for $T > 77$ °K, b in the relation $g \propto J_{nom}^b$ is greater than

1.5 and a change in g or α_l yields a smaller change in J_{nom}.

In the spontaneous emission-spectra measurements, the laser was mounted with n side down on a conventional diode header as shown in Fig. 6 (a). Light emitted from one side of the Fabry-Perot resonator was detected with a Spex-II spectrometer equipped with a type S-1 cathode photomultiplier.[21] The other side of the resonator was coated with a layer of black wax to reduce the portion of the signal due to multiple reflection between two mirrors. The light originating from the p layer and passing through the n layer was either blocked by the diode header or was outside of the detection angle, due to refraction, and was not detected. For the detected signal, it is therefore sufficient to analyze the light entirely coming out from the p region. The lasers were also excited with the same pulse rate and pulse duration as used for the threshold-current measurement. The output of the sampling scope was directly recorded to obtain the spectra. A Tektronix-FET probe was used to match the impedances between the output of the photomultiplier and the input of the scope to improve the signal-to-noise ratio. The final spectra were all corrected for the instrument transmission and photomultiplier response.

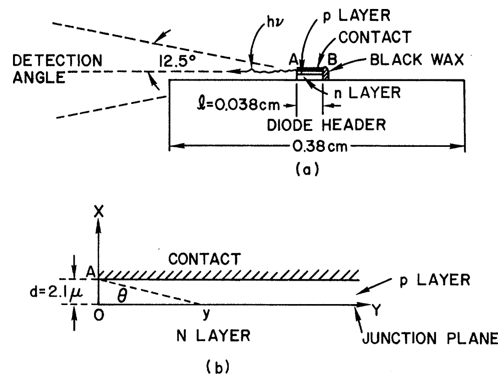

FIG. 6. (a) The schematic diagram for the laser mounting used in the superradiance spectra measurements. (b) The schematic diagram used to analyzing the detected light emerging from one side of the Fabry-Perot resonator.

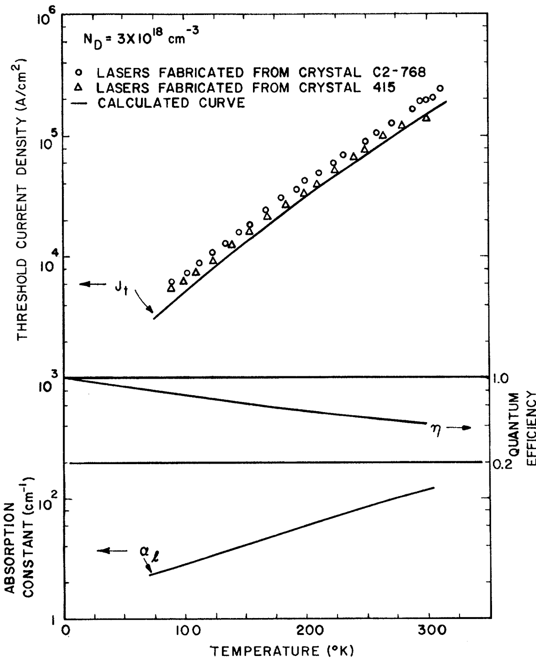

FIG. 5. Comparison of the calculated and experimental temperature dependence of the threshold current. η is taken from Ref. 23. α_l is the measured loss of the lasers defined in Eq. (10). The laser length is 380 μm.

B. Results and Discussions of Comparison

1. *Temperature Dependence of Threshold Current*

Since the diffusion profile is nonuniform, the precise total injection current can only be calculated by solving a diffusion equation with a spatial and concentration-dependent diffusion constant for the electron distribution. This is a rather complicated problem and can not be solved by simple means. Consequently, we shall make the following assumptions. We divide the p region into small subregions with width l_1. In each subregion, the impurity concentration is assumed to be constant and is taken as the average impurity concentration in this subregion. The electron distribution in each subregion is assumed to be of the form

$$N_{i+1}(x-il_1)=N_i(il_1)\,e^{-(x-il_1)/L_{i+1}}, \tag{11}$$

where i is some running index and the subscript denotes the number of the subregion. Thus, $N_1(x)$ which corresponds to $i=0$ refers to the electron concentration at x from the junction in the first subregion next to the junction plane. The diffusion length L_{i+1} is calculated using the average impurity concentration appropriate for the subregion $(i+1)$. Since $L_{i+1}=(D_{i+1}\tau_{i+1})^{1/2}$ and $\tau_{i+1}=\eta N_{i+1}/\mathcal{R}_{i+1}$, the problem of evaluating L_{i+1} reduces to the calculation of D_{i+1} for a given η. The diffusion constant D_{i+1} is calculated from the product of the electron mobility and the carrier diffusion energy defined by Stern.[2] The mobility is obtained by combining the polar mobility and the mobility due to impurity scattering in the relaxation-time approximation, which should be a reasonable one at high impurity concentration.[22] We calculate the mobility due to impurity scattering from a generalized Brooks-Herring-Dingle formula and a quantum correction given by Moore,[22] both of

which can be expressed in terms of carrier screening length. Thus, given η, L_{i+1} can be determined from our previously calculated data without introducing other parameters. Three subregions will be used in the present calculation. It turns out that more subregions essentially yield the same result since in all cases $L_{i+1} > l_1$.

As the applied forward bias is increased, $N_1(0)$ increases. The lasing threshold will be reached at a certain $N_1(0)$ which gives a value of some $N_{i+1}(x - il_1)$ required to maintain a gain equal to the total loss of the laser. From Eqs. (7) and (9), we obtain

$$J_t = \left(\frac{1.602\times 10^{-23}}{\eta\eta_1\Gamma}\right) l_1 \sum_{i=0}^{2} \mathcal{R}_{i+1} \quad . \tag{12}$$

In the upper part of Fig. 5, we plot (solid curve) the calculated J_t as a function of temperature using $\Gamma = 1$; we also plot (middle part of Fig. 5) a temperature dependence of η taken from Pilkuhn and Rupprecht.[23] The use of $\Gamma = 1$ should be reasonable since our lasers were fabricated with a shallow junction and an optimum strip width[24] and we expect to have a better mode confinement than an ordinary laser whose Γ is about 0.9.[25] The experimental values are also plotted as open circles and open triangles for comparison. It is seen that the agreement is reasonably good considering that there are so many quantities and steps involved in the calculation. This result indicates that a number of assumptions made in the calculation may not be too critical. It also shows for the first time a calculated near-exponential temperature dependence of the threshold current. Using the approximation of Eq. (11), we found that the lasing occurs almost simultaneously in subregions 1 and 2 at 300 °K if we assume they have the same α_L. This gives an active region of about 1.5 μ. The same argument shows that the active-region width is about 1 μ at 80 °K. Both of these two values are also in good agreement with experiment.[7,25] We noted that the use of $N_A - N_D = 3\times 10^{18}$ cm^{-3}, in paper I and in Sec. II of this paper, as the average compensation in the active region is more or less justified, even though a value of $N_A - N_D = 2\times 10^{18}$ cm^{-3} would have been more appropriate.

2. *Spontaneous Emission Spectra*

Here, we wish to compare the calculated spontaneous band shape and the relative change of the emission intensity with the injection current with the experimental ones. This calculation is very useful in supporting our calculated densities of state, since the low-energy side of the spectra should reflect the structure of the state density functions. Because the recombination occurs internally in the laser, the reabsorption is important in determining the observed band shape. We refer to Fig. 6 (b) for the analysis of light propagating through the p layer. We take X as the axis perpendicular to the junction plane and Y as the axis on the junction plane, perpendicular to the mirrors. The detection angle is determined by the size of the lens on the far left-hand side (not shown) and is equal to half of the solid angle generated by an angle of 12.5° (the other half is blocked by the diode header). The light emerging from the mirror at $y = 0$ will be detected if the angle of refraction is equal to or smaller than 12.5°. Take, for example, a point y on the Y axis as the point where the recombination takes place. The light within the half solid angle generated by θ will be detected if θ is satisfied by either one or both of the two conditions:

$$\sin 12.5^\circ / \sin\theta \le n = 3.6 \tag{13}$$

and

$$\tan\theta \le d/y = 2.1/y . \tag{14}$$

Denoting y_0 the solution of Eqs. (13) and (14), we find $y_0 = nd/\sin 12.5^\circ = 36\ \mu$. For $y \le y_0$, Eq. (13) has to be satisfied. For $y \ge y_0$, the value of θ has to satisfy Eq. (14). We note that Eqs. (13) and (14) both imply $x \ll y$ for all y. Since the contributions from recombination radiation at different points are incoherent, they are additive. Thus, the total detected light $I(hv, x=0)$ due to recombinations at all points along y axis is

$$I(hv, x=0) = \frac{1-R}{l}\, T\left[\int_0^{y_0} \gamma(hv, x=0)\left(\frac{1}{4\pi}\right)\left(\frac{\pi x^2}{2y^2}\right) e^{-\alpha' y} dy + \int_0^{l} \gamma(hv, x=0)\left(\frac{1}{4\pi}\right)\left(\frac{\pi d^2}{2y^2}\right) e^{-\alpha' y} dy\right] , \tag{15}$$

where T is the transmittance of the light across the boundary between two media with different refraction indices and is nearly independent of θ for $x \ll y$,[26] R is the reflectivity of the mirror, $w^2 = y^2(\sin 12.5^\circ/n)$, and $\alpha' = \alpha(h\nu) + \alpha_l$ is the effective absorption constant of the medium. Since $x \ll y$, and $\alpha(h\nu)$ is not a very sensitive function of x (see, for example, Fig. 7), we may take the absorption constant α in Eq. (15) as $\alpha = \alpha(h\nu, x=0)$. Furthermore, since d is much smaller than the distance between the lens and the laser, the detected light originating from planes at $x \ne 0$ in the p layer is the same as Eq. (15). The total detected light $I(h\nu)$ is then given by the superpositions of Eq. (15) for different x,

$$I(h\nu) = \sum_{i=0}^{2} I_{i+1}(h\nu), \tag{16}$$

where $I_{i+1}(h\nu)$ is given by Eq. (15) with appropriate values of $\gamma(h\nu)$ and $\alpha(h\nu)$ for the $i+1$ subregion.

The results calculated from Eqs. (15) and (16) are compared with experimental ones taken near the threshold at 300 °K. It is appropriate to compare our results with the high-bias data for the following reasons. First, it has been shown[27] that at low temperatures ($\lesssim 77$ °K) appreciable radiative tunneling can persist up to a very high bias close to the built-in voltage of the diode. Second, appreciable tunneling exists at 255 °K when the forward bias is low.[27] It is thus clear that the spontaneous-emission spectrum, particularly the low-energy side of the band, at low or at high temperatures and low bias will not give information on the structure of the density of states in the active region. We therefore use 300 °K superradiance spectra in order to minimize the contribution from the radiative tunneling. In Fig. 8, we plot the calculated spontaneous spectra in the vicinity of the threshold, as indicated by the parameter r which denotes the ratio of the current density to the threshold-current density:

$$r = \sum_{i=0}^{2} \mathcal{R}_{i+1} \Big/ \sum_{i=0}^{2} (\mathcal{R}_{i+1})_{N(0)=N_t(0)} , \tag{17}$$

where $N(0) = N_t(0)$ means that the $\mathcal{R}$'s are evaluated at the value of $N(0)$ which would make the diode lase if one side of the diode were not coated with the black wax. The experimental spectra are also plotted as points for comparison. It is seen that, except for the peak positions of the spectra, the calculated and experimental data show good agreement both in the band shape and in the change of intensity with the injection current. The disagreement in the peak position, which is about 5 meV in this case, reflects the uncertainty in the band-gap energy as discussed in paper I. However, the change of 5 meV in energy yields less than 5% error in the calculated absorption constant.

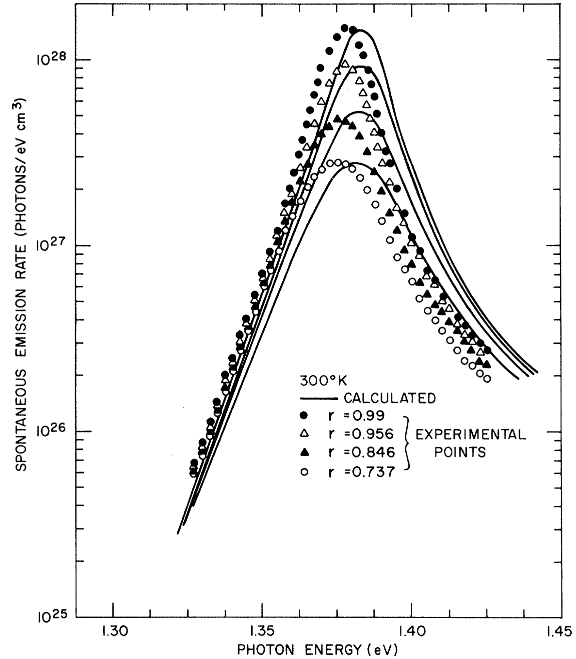

FIG. 8. Comparison of the calculated and experimental superradiance spectra at 300 °K for a diffused junction laser with 3×10^{18} cm^{-3} substrate doping. The injection level is denoted by r which is defined as the ratio of the injection current to the threshold current.

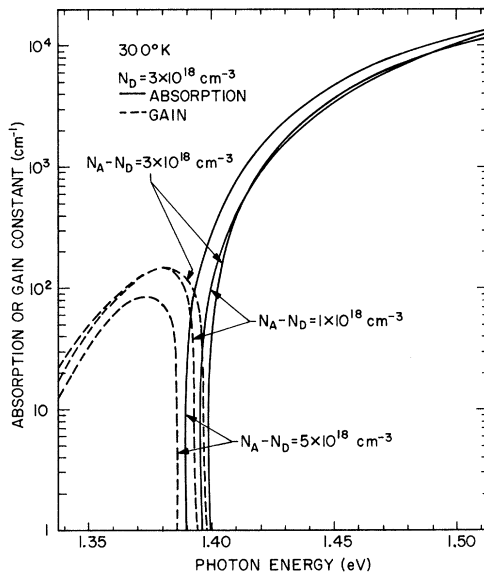

FIG. 7. The absorption and gain spectra at the lasing threshold at 300 °K in the p layer for a diffused junction laser with 3×10^{18} substrate doping.

The good agreement between the calculated and experimental spectra adds support to our conclusion of a negligibly small conduction band tail. Consequently, the shape of the low-energy side of the electroluminescence band at high-forward bias should be largely a measure of the valence band tail in the active region rather than the conduction band tail, as assumed in most of the previous work.

IV. SUMMARY OF PAPER I AND PAPER II

The temperature dependence of the threshold current and the superradiance spectra have been calculated for a GaAs junction laser by computing the spontaneous and stimulated spectral functions. These require a knowledge of the density of states and the matrix element for the optical transitions. The form of the density of states adopted consists of a tail part, given by Halperin and Lax, and an ordinary effective-mass parabolic band. The use of the unperturbed parabolic band is justified since calculations using perturbation techniques show

negligible distortion of the band in this region. The parameters associated with the densities of states are then determined self-consistently. It is found that in the active region of a typcial GaAs junction laser the conduction band tail is negligibly small compared with the valence band tail. This observation is contrary to both the generally accepted assumption and Stern's calculation, using Kane's density of states of a long and reasonable large conduction band tail. On the basis of the present calculation, it is concluded that the electron quasi-Fermi level at threshold for a typical laser, at temperature above 77 °K, should be in the parabolic portion of the band, and that the frequent assumption for the location of the electron quasi-Fermi level in the conduction band tail is not justified.

The self-consistent densities of states are then used to calculate the spontaneous and stimulated absorption spectral functions by using an optical model with an energy-dependent matrix element and no selection rule for the radiative transitions. This matrix element is that which is appropriate for the average conduction band to acceptor level transitions; and it should be a reasonable one to use, since our conduction band tail is negligibly small, and most of the hole population is in the energy range close to the acceptor ionization energy. Our calculated general properties of the spontaneous and stimulated emission are different from that obtained by using a parabolic or Kane's density of states. The calculations on the temperature dependence of the threshold current and the superradiance spectra have been applied to diffused GaAs diodes with substrate doping of 3×10^{18} cm^{-3} , by taking into account the temperature dependence of the cavity loss and the nonuniform distribution of the acceptors. Detailed comparison with experimental data have been made and good quantitative agreements are found.

ACKNOWLEDGMENTS

I wish to thank R. L. Brown for computer programming. I am also indebted to Dr. F. Stern, Dr. E. C. Lightowlers, Dr. E. O. Kane, and Dr. H. C. Casey, Jr.,for valuable comments.

[1]C. J. Hwang, preceeding paper, Phys. Rev. B 2, 4117 (1970).
[2]F. Stern, Phys. Rev. 148, 186 (1966).
[3]G. Lasher and F. Stern, Phys. Rev. 133, A553 (1964).
[4]W. P. Dumke, Phys. Rev. 132, 1998 (1963).
[5]K. Unger, Z. Physik 207, 322 (1967).
[6]K. Unger, Z. Physik 207, 332 (1967).
[7]See, for example, M. H. Pilkuhn, H. Rupprecht, and S. Blum, Solid-State Electron. 7, 905 (1964).
[8]W. Susaki, T. Oku, and T. Sogo, IEEE J. Quantum Electron. QE-4, 122 (1968).
[9]A. R. Goodwin, Solid State Device Research Conference, Rochester, 1969 (unpublished).
[10]G. E. Pikus, Fiz. Tverd. Tela 7, 3536 (1965) [Soviet Phys. Solid State 7, 2854 (1966)].
[11]J. C. Dyment (private communication).
[12]J. I. Pankove, IEEE J. Quantum Electron. QE-4, 119 (1968).
[13]K. K. Shih, J. W. Allen, and G. L. Pearson, J. Phys. Chem. Solids 29, 367 (1968).
[14]K. K. Shih, J. W. Allen, and G. L. Pearson, J. Phys. Chem. Solids 29, 379 (1968).
[15]L. L. Chang and G. L. Pearson, J. Phys. Chem. Solids 25, 23 (1964).
[16]H. C. Casey, Jr., M. B. Panish, and L. L. Chang, Phys. Rev. 162, 660 (1967).
[17]R. Sh. Malkovich and G. K. Malysh, Fiz. Tverd. Tela. 9, 553 (1967) [Soviet Phys. Solid State 9, 423 (1967)].
[18]M. Fujimoto, Y. Sato, and K. Kudo, Japan J. Appl. Phys. 6, 848 (1967).
[19]J. C. Dyment, Appl. Phys. Letters 10, 84 (1967).
[20]I am indebted to J. C. Dyment for permission to use this data.
[21]C. J. Hwang, J. Appl. Phys. 38, 4811 (1967); 39, 1654 (1968).
[22]E. J. Moore, Phys. Rev. 160, 618 (1967).
[23]M. Pilkuhn and H. Rupprecht, J. Appl. Phys. 38, 5 (1967).
[24]J. C. Dyment, J. E. Ripper, and T. H. Zachos, J. Appl. Phys. 40, 1802 (1969).
[25]F. Stern, in *Physics of III-V Compounds*, edited by R. K. Willardson and A. C. Beer (Academic, New York, 1966), Vol. II, p. 371.
[26]J. Vilms and W. E. Spicer, J. Appl. Phys. 36, 2815 (1965).
[27]H. C. Casey and D. J. Silversmith, J. Appl. Phys. 40, 241 (1969).